Journal of Hepatocellular Carcinoma

Dovepress

open access to scientific and medical research

Open Access Full Text Article

ORIGINAL RESEARCH

Exploring the MRI and Clinical Features of P53-Mutated Hepatocellular Carcinoma

Jingfei Weng[1,2,*], Yuyao Xiao[1,*], Jing Liu[3,*], Xiaohua Liu[4], Yuqing He[2], Fei Wu[1], Xiaoyan Ni[1], Chun Yang[1]

[1]Department of Radiology, Zhongshan Hospital, Fudan University, Shanghai, People's Republic of China; [2]Department of Radiology, The Affiliated Traditional Chinese Medicine Hospital, Southwest Medical University, Luzhou, People's Republic of China; [3]Department of Radiology, Fudan University Shanghai Cancer Center, Shanghai, People's Republic of China; [4]Department of Radiology, The Affiliated Hospital of Xuzhou Medical University, Xuzhou, People's Republic of China

*These authors contributed equally to this work

Correspondence: Chun Yang; Xiaoyan Ni, Department of Radiology, Zhongshan Hospital, Fudan University, Shanghai, People's Republic of China, Tel +86 18702135336; +86 15201803582, Email dryangchun@hotmail.com; nixiaoyan1103@126.com

Purpose: To study the MRI features (based on LI-RADS) and clinical characteristics of P53-mutated hepatocellular carcinoma (HCC) patients.

Patients and Methods: This study enrolled 344 patients with histopathologically confirmed HCC (P53-mutated group [n = 196], non-P53-mutated group [n = 148]). We retrospectively evaluated the preoperative MRI features, clinical and pathologic features of the lesions and assigned each lesion according to the LI-RADS. MRI findings, clinical features, and pathologic findings were compared using the Student's t test, $\chi 2$ test, and multivariable regression analysis.

Results: Most HCC patients were categorized as LR-5. On multivariate analysis, the Edmondson–Steiner grade (odds ratio, 2.280; 95% CI: 1.268, 4.101; $p = 0.006$) and rim enhancement (odds ratio, 2.517; 95% CI: 1.095, 5.784; $p = 0.030$) were found to be independent variables associated with P53-mutated HCC. In the group of HCC lesions with the largest tumor diameter (LTD) greater than or equal to 10mm and less than or equal to 20mm, enhancing capsule was an independent predictor of P53-mutated HCC (odds ratio, 6.200; 95% CI: 1.116, 34.449; $p = 0.037$). Among the HCC lesions (20 mm < LTD ≤ 50 mm), corona enhancement (odds ratio, 2.102; 95% CI: 1.022, 4.322; $p = 0.043$) and nodule-in-nodule architecture (odds ratio, 2.157; 95% CI: 1.033, 4.504; $p = 0.041$) were found to be independent risk factors for P53 mutation. Among the HCC lesions (50 mm < LTD ≤ 100 mm), diameter (odds ratio, 1.035; 95% CI: 1.001, 1.069; $p = 0.044$) and AFP ≥ 400 (ng/mL) (odds ratio, 3.336; 95% CI: 1.052, 10.577; $p = 0.041$) were found to be independent variables associated with P53-mutated HCC.

Conclusion: Poor differentiation and rim enhancement are potential predictive biomarkers for P53-mutated HCC, while HCCs of different diameters have different risk factors for predicting P53 mutations.

Keywords: liver neoplasms, magnetic resonance imaging, P53-mutated

Introduction

More than 90% of primary liver cancers are hepatocellular carcinoma (HCC) and are predisposed to occur in patients with underlying chronic liver disease.[1] HCC has a high mortality rate, and the survival rate of patients with advanced HCC is very low.[2] HCC has a poor prognosis mainly because it is prone to vascular infiltration, metastasis and recurrence.[3] It is important for patients to be able to make preoperative predictions about the prognosis of hepatocellular carcinoma and to choose appropriate treatment options. Therefore, additional data about the pathogenesis of HCC are needed to investigate new and more effective treatments to improve the survival of HCC patients.

P53 is an important tumor suppressor gene involved in the development of hepatocellular carcinoma, and it is closely related to cell cycle arrest, cellular regulation and cellular senescence.[4] While the wild-type P53 gene is a tumor suppressor gene, mutant P53 has oncogenic activity, this protein not only binds to wild-type P53 to form a complex

Received: 9 March 2024
Accepted: 1 August 2024
Published: 29 August 2024

and inhibit P53 gene function but also promotes abnormal cell proliferation and participates in tumor formation.[5] The most commonly mutated genes in hepatocellular carcinoma are *TERT* (promoter), *TP53, CTNNB1, AXIN1, ARID1A*, and *ARID2*, whereas the chance of mutation occurring in other genes is less than 10%.[6] Enrichment of *TP53* inactivating mutations promotes the onset of HCC proliferation, including in clinically aggressive tumors with poor differentiation and frequent vascular invasion. The mutation rate of the P53 gene in HCC patients is 31.5%, and the expression up-regulation is 35.0%. Moreover, P53 expression can lead to a poor prognosis in HCC patients.[7]

Small HCCs with a diameter of ≤2 cm have low invasiveness, but their incidence is increasing annually, and the optimal treatment options are uncertain. Small-diameter (less than 2 cm) HCCs have high resection rates and low recurrence rates.[8] Liver transplantation is the best therapeutic option for patients with unresectable HCC. The Milan criterion for liver transplantation is a single nodule ≤5 cm in length.[9] Mazzaferro et al[10] reported that among patients who had undergone liver transplantation for HCC, the 4-year recurrence-free survival rate was 83%, and the ability of patients to choose the right treatment helped improve their survival. Liver transplantation also has some limitations in that it mainly selects HCC that meets the Milan criteria, and overall survival remains low for out-of-criteria HCC and patients with high-risk HCC features (with microvascular invasion and poorly differentiated tumors).[11]

P53-mutated HCC is a major subtype of HCC, and the ability to identify P53-mutated HCC in a noninvasive manner can help patients develop a personalized treatment plan. Several studies have shown that P53-mutated HCC is associated with dilated vasculature in the arterial phase and a decreased relative enhancement ratio in the hepatobiliary phase of gadoxetic acid–enhanced MRI;[12] however, imaging manifestations in the ancillary features of HCC (mosaic architecture, nodule-in-nodule architecture, etc.) have not been investigated, and their diameters have not been further categorized. Therefore, we investigated the imaging features of HCCs expressing P53 mutations on contrast-enhanced MR and explored whether there were differences in the imaging features of P53-mutated HCCs with different diameters.

Materials and Methods

Patient Selection

The study was approved by the institutional review board committees of Zhongshan Hospital, Fudan University (approval number: B2021–113R), and patient informed consent was waived. Our study was retrospective and therefore consent was waived. Our study covers patient data confidentiality and compliance with the Declaration of Helsinki. Between January 2020 and December 2020, a total of 910 consecutive patients were confirmed to have HCC by postoperative pathology with P53 immunohistochemistry and no extrahepatic metastases on preoperative examination. The inclusion criteria were (a) primary liver lesion without any previous treatment; (b) MRI examination within 30 days before the operation, for which the MRI scan was clear and suitable for diagnosis; (c) a single mass; and (d) a maximum lesion diameter between 10 mm and 100 mm. Finally, 566 patients were excluded for the following reasons: lack of clinical data (n = 15); history of previous treatment, including surgery and transarterial chemoembolization (TACE) therapy (n = 242); lack of MRI data available 1 month before the procedure or poor MRI images, which made it difficult to make a diagnosis (n = 32); two or more HCC lesions in the same liver (n = 178); and lesions with a maximum diameter less than 10 mm or more than 100 mm (n = 99), because the imaging signs of larger tumors are complex in presentation and affect the judgement of the results. Finally, 344 patients with HCC were enrolled in this study (Figure 1).

Histologic Diagnosis and Immunohistochemistry

Pathologic analyses, including immunohistochemistry, revealed the following features: tumor differentiation according to the Edmondson–Steiner grade and the presence of microvascular or macrovascular invasion. Immunohistochemistry for P53 was performed for all 344 patients with HCC, and then the patients were classified into P53-mutated HCC and non-P53-mutated HCC groups. P53 expression in tumor tissue was scored according to the percentage of cells exhibiting positive nuclear staining; P53 expression was defined as positive when 10% or more of the cells exhibited nuclear staining.[13]

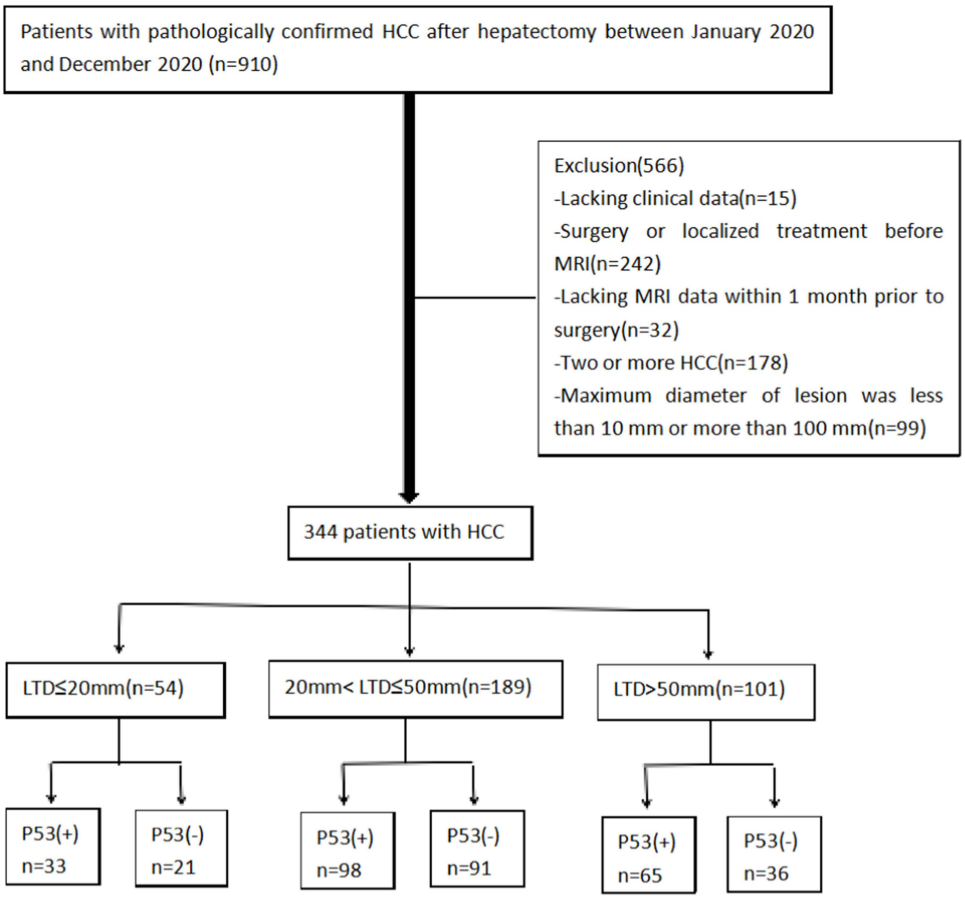

Figure 1 Patient selection process and exclusion criteria.
Abbreviations: HCC, hepatocellular carcinoma; MRI, magnetic resonance imaging; LTD, the largest tumor diameter; P53(+), P53-mutated; P53(-), non-P53-mutated.

MRI Technique

All patients were examined Gd-DTPA enhanced liver MRI. Patients were scanned using the following nine MRI scanners: a Magnetom Aera 1.5T imager (Siemens Healthcare, Erlangen, Germany) for 55 patients; a 3.0T UIHMR770 scanner (United Imaging Healthcare, Shanghai, China) for 102 patients; a Magnetom Avanto 1.5T imager (Siemens Healthcare, Erlangen, Germany) for 44 patients; a 1.5T UIHMR560 scanner (United Imaging Healthcare, Shanghai, China) for 76 patients; and a Magnetom Verio 3.0T MRI System (Siemens Healthcare, Erlangen, Germany) for 14 patients; a Prisma 3.0T MRI System (Siemens Healthcare, Erlangen, Germany) was used for 26 patients, and Ingenia CX3.0 MRI System (Philips Medical Systems, Best, the Netherlands) for 27 patients. Gd-DTPA was intravenously administered at a rate of 2 mL/s for a total dose of 0.1 mmol/kg. The routine MR imaging protocol included transverse T2-weighted breath-hold fat-suppressed fast spin–echo sequence, T1-weighted breath-hold in-phase and opposed-phase gradient echo sequence, and free-breath diffusion-weighted imaging (DWI) with a transverse single-shot spin–echo planar sequence (b value, 0, 50, and 500 s/mm^2). The contrast-enhanced MR imaging protocol included pre- and postcontrast three-dimensional T1-weighted imaging in the arterial phase (20–30 s), portal venous phase (70–90 s) and delayed phase (160–180 s).

Imaging Analyses

Images were analysed by two radiologists (** and ** with 9 and 16 years of abdominal imaging analysis experience, respectively) retrospectively. If there was an inconsistency between the two radiologists, a consensus was reached through discussion. The following findings were assessed Gd-DTPA enhanced MRI (Figures 2–4): (a) enhancement patterns (hypoenhanced-isoenhanced, nonrim arterial phase hyperenhancement and rim enhancement); (b) washout

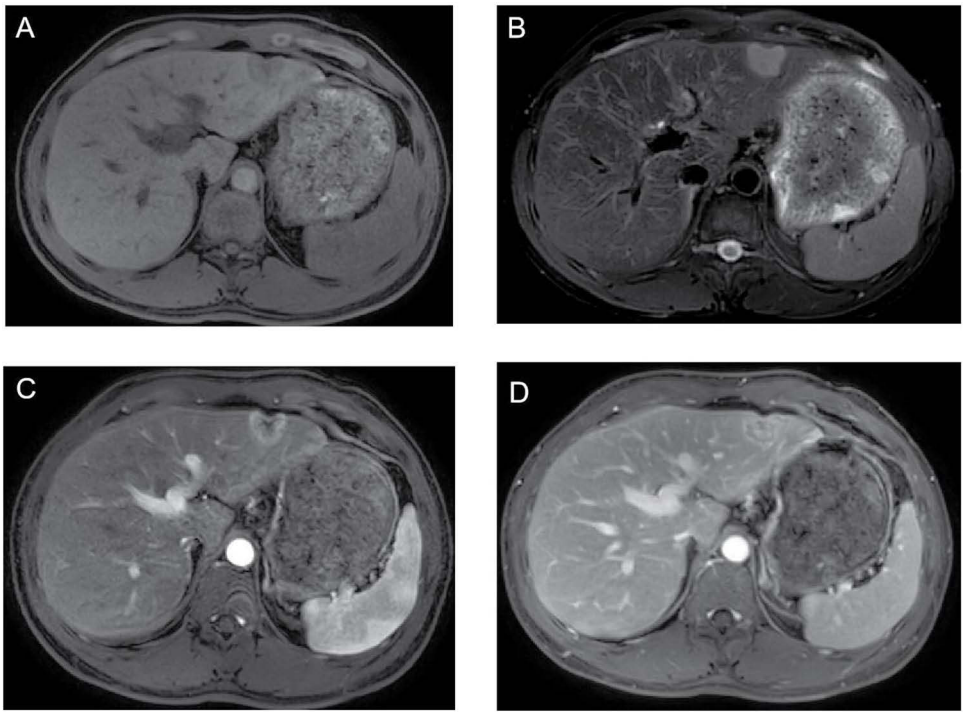

Figure 2 Images in a 40-year-old man with P53-mutated HCC; the serum level of AFP was 4.2 ng/mL. (**A**) T1-weighted image shows a 27mm hypointense mass. (**B**) T2-weighted image shows a hyperintense mass. (**C**) Axial arterial phase image shows a rim enhancement mass. (**D**) Delayed phase image shows delayed enhancement in the center of the mass.

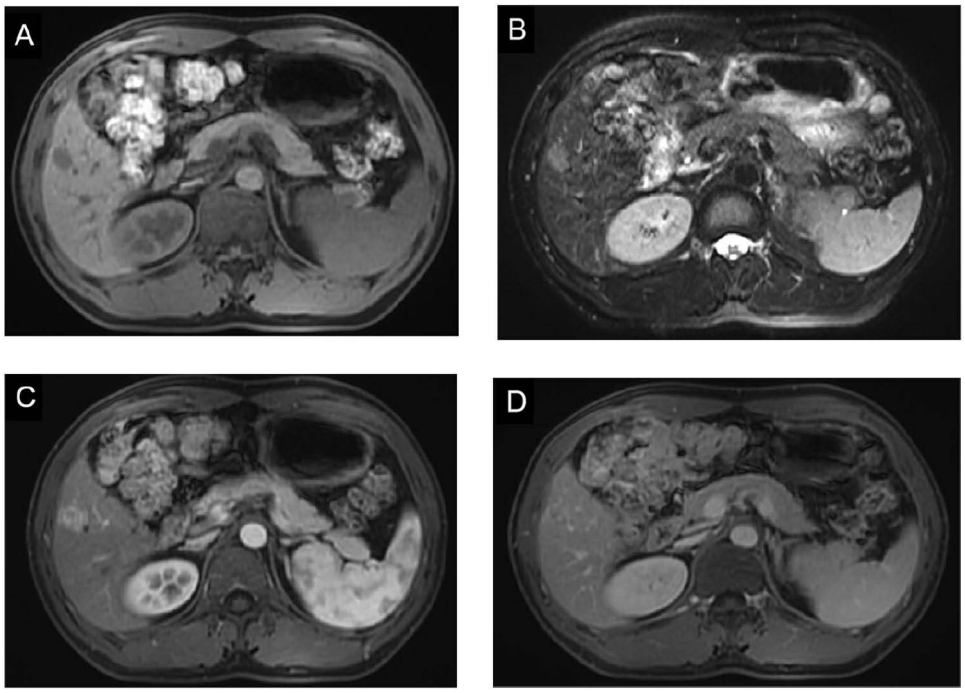

Figure 3 Images in a 38-year-old man with P53-mutated HCC; the serum level of AFP was 3.6 ng/mL. (**A**) T1-weighted image shows a 17mm hypointense mass. (**B**) T2-weighted image shows a hyperintense mass. (**C**) Axial arterial phase image shows a hypervascular mass. (**D**) Delayed phase image shows a mass with enhancing capsule.

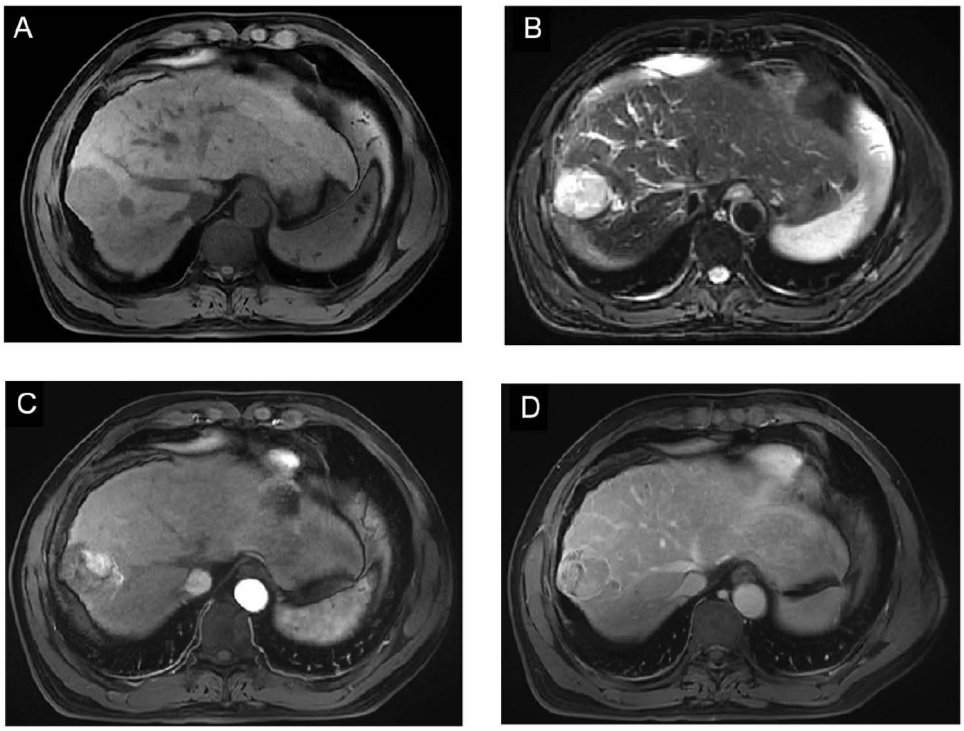

Figure 4 Images in a 50-year-old man with P53-mutated HCC; the serum level of AFP was 11.4 ng/mL. (**A**) T1-weighted image shows a 42mm hypointense mass. (**B**) T2-weighted image shows a hyperintense mass. (**C**) Axial arterial phase image shows a mass with nodule-in-nodule architecture and irregular peritumoral enhancement. (**D**) Delayed phase image shows nodule-in-nodule architecture washout and peritumoral slight hypointensity.

patterns (no washout, nonperipheral washout, peripheral washout); (c) dilated vasculature, defined as thick branching vessels of similar contrast to arteries with a maximum diameter >2 mm; (d) delayed central enhancement, defined as progressive enhancement in the central region of the lesion in the delayed phase; (e) enhancing capsule, defined as an enhancing rim of tissue that appears during the portal venous and delayed phases; (f) corona enhancement, defined as periobservation enhancement in the late arterial or early portal venous phase; (g) mosaic architecture, defined as randomly distributed internal nodules or compartments on T2WI images; and (h) nodule-in-nodule architecture, defined as a mass with a smaller internal nodule within a larger nodule accompanied by marked enhancement in the arterial phase with washout in the portal phase. (i) A tumor in the vein was defined as an occluded vein adjacent to the intrahepatic mass. In addition, intratumoral hemorrhage, fat deposition, restriction diffusion status (yes or not), and hepatic capsule retraction were also assessed.

Clinical Data

Clinical information such as age, sex, background liver characteristics, liver functional parameters, and serum tumor marker levels of AFP, CA19–9, and CEA was collected.

Statistical Analysis

All statistical analyses were performed using SPSS 26.0. Inter-reader agreement was expressed by Cohen's kappa coefficient. A kappa statistic of 0.81–1.0 was considered very good, 0.61–0.80 was considered good agreement, 0.41–0.60 was considered moderate agreement, 0.21–0.40 was considered fair agreement, and 0–0.20 was considered poor agreement. Continuous variables were compared using Student's *t* test, and categorical variables were compared among different groups using the $\chi 2$ test or Fisher's exact test. Parameters were analysed using univariate and multivariate logistic regression to determine whether they were independent risk factors for P53-mutated HCC. Univariate analyses were performed first, and only those parameters found to be statistically significant ($p < 0.05$) were used in stepwise multivariate logistic regression.

Results

Patient Clinical

In our study, a total of 344 patients were included, 196 cases (57.0%) were P53-mutated HCC and 148 cases (43.0%) were non-P53-mutated HCC, of which 54 cases had HCC with a maximum diameter of 10 mm to 20 mm, 33 cases (61.1%) were P53 mutated and 21 cases (38.9%) were non-mutated; 189 cases had HCC with a maximum diameter of 20 mm to 50 mm, 98 cases (51.8%) were P53 mutated and 91 cases (48.1%) were non-mutated; and 101 cases had HCC with a maximum diameter of 50 mm to 100 mm, 65 cases (64.4%) were P53 mutated and 36 cases (35.6%) were non-mutated.

There were significant differences in the largest tumor diameter, AFP level, Edmondson–Steiner grade and microvascular invasion between P53-mutated HCC patients and non-P53-mutated HCC patients ($p = 0.018$, $p = 0.012$, $p < 0.001$ and $p = 0.034$, respectively; Table 1). In patients with HCC with a diameter greater than or equal to 10mm and less than or equal to

Table 1 Clinical Characteristics HCC According to P53 (10mm ≤ LTD ≤ 100mm)

Clinical parameters	Non-P53-mutated (n = 148)	P53-mutated (n = 196)	*p* value
Age (years)[a]	59.26±11.68	57.27±11.22	0.109
Sex (male:female)	116:32	163:33	0.262
Largest diameter (mm)[a]	39.09±18.39	44.52±23.76	0.018
Etiology[†]			0.939
Hepatitis A virus	1(0.7)	1(0.5)	
Hepatitis B virus	107(72.3)	146(74.5)	
Hepatitis C virus	1(0.7)	2(1.0)	
None or other	39(26.4)	47(24.0)	
Liver functional parameters			
Total bilirubin > 20 (μmol/L)	25(16.9)	29(14.8)	0.597
Direct bilirubin > 7 (μmol/L)	13(8.8)	17(8.7)	0.971
Alanine aminotransferase > 40 (IU/L)	33(22.3)	42(21.4)	0.847
Aspartate aminotransferase > 40 (IU/L)	25(16.9)	37(18.9)	0.635
γ-Glutamyltranspeptidase > 60 (IU/L)	44(29.7)	52(26.5)	0.513
Alpha-fetoprotein			0.012
Alpha-fetoprotein < 20(ng/ml)	82(55.4)	89(45.6)	
Alpha-fetoprotein ≥ 20 and < 400 (ng/ml)	43(29. 1)	49(25. 1)	
Alpha-fetoprotein ≥ 400 (ng/ml)	23(15.5)	57(29.2)	
Cancer antigen 19-9 > 37 (U/ml)	21(15.2)	20(10.9)	0.247
Carcinoembryonic antigen > 5 (ng/ml)	11(7.4)	11(5.6)	0.495
Edmondson-Steiner grade (II:III)	126:22	135:61	<0.001
Microvascular invasion	44(29.7)	80(40.8)	0.034

Notes: Data are numbers of patients (percentage), unless otherwise specified. [a]Data are means ± standard deviations. [†]Data were compared using the Fisher's exact test. The ages were compared using an independent sample *t* test. Excepted where indicated, data were compared using the $\chi 2$ test.

20 mm, there were no significant differences in age, sex, diameter, etiology, liver function parameters, AFP, CA 19–9, CEA levels, Edmondson–Steiner grade, or microvascular invasion ($p > 0.05$; Table 2). In patients with HCC with a diameter greater than 20 mm and less than or equal to 50 mm, there were significant differences in the Edmondson–Steiner grade between P53-mutated HCC and non-P53-mutated HCC ($p = 0.023$; Table 3). Among patients with HCC with a diameter greater than 50 mm and less than or equal to 100 mm, P53-mutated HCC had greater maximum diameters and serum AFP levels than non-P53-mutated HCC ($p = 0.011$ and $p = 0.008$, respectively; Table 4).

Imaging Features

The interobserver agreement for MRI features was good, with a kappa coefficient ranging from 0.704 to 0.958 (Table 5).

There were significant differences in hepatic capsule retraction and corona enhancement between P53-mutated HCC patients and non-P53-mutated HCC patients ($p = 0.047$ and $p = 0.021$, respectively; Table 6). Among the groups with a diameter greater than or equal to 10mm and less than or equal to 20 mm, the P53-mutated group was more likely to have an enhancing capsule than the non-mutated group ($p = 0.045$), and hemorrhage, fat, rim enhancement, mosaic

Table 2 Clinical Characteristics HCC According to P53 (10mm ≤LTD ≤ 20mm)

Clinical parameters	Non-P53-mutated (n = 21)	P53-mutated (n = 33)	*p* value
Age (years)[a]	57.62±11.50	54. 12±8.88	0.215
Sex (male:female)	14:7	27:6	0.204
Largest diameter (mm)[a]	16.57±2.94	16. 15±2.76	0.598
Etiology[†]			0.557
Hepatitis B virus	16(76.2)	28(84.8)	
Hepatitis C virus	1(4.8)	0(0)	
None or other	4(19.0)	5(15.2)	
Liver functional parameters			
Total bilirubin > 20 (μmol/L)[†]	2(9.5)	5(15.2)	0.693
Direct bilirubin > 7 (μmol/L)[†]	1(4.8)	3(9. 1)	1.000
Alanine aminotransferase > 40 (IU/L)[†]	2(9.5)	5(15.2)	0.693
Aspartate aminotransferase > 40 (IU/L)[†]	2(9.5)	1(3.0)	0.553
γ-Glutamyltranspeptidase > 60 (IU/L)[†]	2(9.5)	3(9. 1)	1.000
Alpha-fetoprotein[†]			0.598
Alpha-fetoprotein < 20(ng/ml)	12(57. 1)	14(42.4)	
Alpha-fetoprotein ≥ 20 and < 400 (ng/ml)	6(28.6)	14(42.4)	
Alpha-fetoprotein ≥ 400 (ng/ml)	3(14.3)	5(15.2)	
Cancer antigen 19-9 > 37 (U/ml)[†]	3(14.3)	2(6. 1)	0.366
Carcinoembryonic antigen > 5 (ng/ml)[†]	1(4.8)	2(6. 1)	1.000
Edmondson-Steiner grade (II:III)[†]	20:1	24:9	0.69
Microvascular invasion[†]	0(0)	6(18.4)	0.071

Notes: Data are numbers of patients (percentage), unless otherwise specified. [a]Data are means ± standard deviations. [†] Data were compared using the Fisher's exact test. The ages were compared using an independent sample *t* test. Excepted where indicated, data were compared using the χ2 test.

Table 3 Clinical Characteristics HCC According to P53 (20mm < LTD ≤ 50mm)

Clinical parameters	Non-P53-mutated (n =91)	P53-mutated (n =98)	*p* value
Age (years)[a]	58.67±11.71	58.31±11.85	0.832
Sex (male:female)	74:17	80:18	0.956
Largest diameter (mm)[a]	33.91±8.09	35.19±8.85	0.301
Etiology[†]			0.432
Hepatitis A virus	1(1.1)	1(1)	
Hepatitis B virus	65(71.4)	75(76.5)	
Hepatitis C virus	0(0)	2(2.0)	
None or other	25(27.5)	20(20.4)	
Liver functional parameters			
Total bilirubin > 20 (μmol/L)	16(17.6)	16(16.3)	0.818
Direct bilirubin > 7 (μmol/L)	8(8.8)	9(9.2)	0.925
Alanine aminotransferase > 40 (IU/L)	21(23.1)	16(16.3)	0.243
Aspartate aminotransferase > 40 (IU/L)	10(11.0)	15(15.3)	0.381
γ-Glutamyltranspeptidase > 60 (IU/L)	25(27.5)	16(16.3)	0.063
Alpha-fetoprotein			0.378
Alpha-fetoprotein< 20(ng/ml)	52(57.1)	50(51.5)	
Alpha-fetoprotein ≥ 20 and < 400 (ng/ml)	24(26.4)	23(23.7)	
Alpha-fetoprotein ≥ 400 (ng/ml)	15(16.5)	24(24.7)	
Cancer antigen 19-9 > 37 (U/ml)	10(11.0)	11(11.2)	0.959
Carcinoembryonic antigen > 5 (ng/ml)	6(6.6)	6(6.1)	0.894
Edmonson-Steiner grade (II:III)	76:15	68:30	0.023
Microvascular invasion	26(28.6)	33(33.7)	0.449

Notes: Data are numbers of patients (percentage), unless otherwise specified. [a]Data are means ± standard deviations. [†]Data were compared using the Fisher's exact test. The ages were compared using an independent sample *t* test. Excepted where indicated, data were compared using the $\chi 2$ test.

Table 4 Clinical Characteristics HCC According to P53 (50mm < LTD ≤ 100mm)

Clinical Parameters	Non-P53-Mutated (n = 36)	P53-Mutated (n = 65)	*p* value
Age (years)[a]	61.72±11.65	57.29±11.16	0.063
Sex (male:female)	28:8	56:9	0.281
Largest diameter (mm)[a]	65.33±12.85	72.98±15.03	0.011
Etiology			0.530
Hepatitis B virus	26(72.2)	43(66.2)	
None or other	10(27.8)	22(33.8)	

(*Continued*)

Table 4 (Continued).

Clinical Parameters	Non-P53-Mutated (n = 36)	P53-Mutated (n = 65)	*p* value
Liver functional parameters			
Total bilirubin > 20 (μmol/L)	7(19.4)	8(12.3)	0.334
Direct bilirubin > 7(μmol/L)[†]	4(11.1)	5(7.7)	0.718
Alanine aminotransferase > 40 (IU/L)	10(27.8)	21(32.3)	0.636
Aspartate aminotransferase > 40 (IU/L)	13(36.1)	21(32.3)	0.698
γ-Glutamyltranspeptidase > 60 (IU/L)	17(47.2)	33(50.8)	0.733
Alpha-fetoprotein			0.008
Alpha-fetoprotein< 20(ng/mL)	18(50.0)	25(38.5)	
Alpha-fetoprotein ≥ 20 and < 400 (ng/ml)	13(36. 1)	12(18.5)	
Alpha-fetoprotein ≥ 400 (ng/ml)	5(13.9)	28(43. 1)	
Cancer antigen 19-9 > 37 (U/ml)	8(22.2)	7(10.8)	0. 121
Carcinoembryonic antigen > 5 (ng/ml)[†]	4(11. 1)	3(4.6)	0.244
Edmondson-Steiner grade (II:III)	30:6	43:22	0.065
Microvascular invasion	18(50.0)	41(63. 1)	0.202

Notes: Data are numbers of patients (percentage), unless otherwise specified. [a]Data are means ± standard deviations. [†] Data were compared using the Fisher's exact test. The ages were compared using an independent sample *t* test. Excepted where indicated, data were compared using the χ2 test.

Table 5 Interobserver Agreement of MRI Imaging Features

MRI Features	Kappa value
Enhancement at AP	0.732
Dilated vasculature at AP dynamic MRI	0.958
Washout at portal venous phase	0.806
Delayed central enhancement	0.704
Enhancing capsule	0.917
Corona enhancement	0.852
Mosaic architecture	0.825
Nodule-in-nodule architecture	0.767
Tumor in vein	0.714
LI-RADS	0.762

Abbreviations: AP, arterial phase; MRI, magnetic resonance imaging; LI-RADS, Liver Imaging Reporting and Data System.

architecture, nodule-in-nodule architecture, and LI-M were more likely to occur in the P53-mutated group, however, there was no statistically significant difference in the *p* value ($p > 0.05$; Table 7). In the 20 mm to 50 mm diameter group, the P53-mutated group had a higher incidence of corona enhancement and nodule-in-nodule architecture ($p = 0.023$ and

Table 6 Comparison of Qualitative Data Obtained on MRI Features Stratified by P53 Status (10mm ≤ LTD ≤ 100mm)

MRI Features	Non-P53-Mutated (n =148)	P53-Mutated (n =196)	*p* value
Hypointense at T1-weighted imaging	139(93.9)	190(96.9)	0.174
Mild-moderate hyperintensity at T2-weighted imaging[†]	145(98.0)	191(97.4)	1.000
Hepatic capsule retraction	4(2.7)	15(7.7)	0.047
Hemorrhage	34(23.0)	54(27.6)	0.335
Fat deposition	48(32.4)	73(37.2)	0.355
Diffusion restriction	141(95.3)	186(94.9)	0.875
Enhancement at AP[†]			0.116
Nonrim enhancement	135(91.2)	165(84.2)	
Rim enhancement	9(6.1)	25(12.8)	
Hypoenhanced-isoenhanced	4(2.7)	6(3.1)	
Dilated vasculature at AP dynamic MRI	88(59.5)	112(57.1)	0.666
Washout at portal venous phase			0.962
Nonperipheral washout	117(79.1)	153(78.1)	
Peripheral washout	6(4.1)	9(4.6)	
No washout	25(16.9)	34(17.3)	
Delayed central enhancement	14(9.5)	13(6.6)	0.334
Enhancing capsule	130(87.8)	181(92.3)	0.160
Corona enhancement	31(20.9)	63(32. 1)	0.021
Mosaic architecture	89(60. 1)	129(65.8)	0.279
Nodule-in-nodule architecture	26(17.6)	44(22.4)	0.266
Tumor in vein	5(3.4)	13(6.6)	0.180
LI-RADS†			0.204
LR-3	5(3.4)	2(1.0)	
LR-4	6(4. 1)	11(5.6)	
LR-5	111(75.0)	133(67.9)	
LR-M	21(14.2)	37(18.9)	
LR-TIV	5(3.4)	13(6.6)	

Notes: The data are presented as the number (%) of patients. [†]Data were compared using the Fisher's exact test. LR-3 intermediate probability for malignancy, LR-4 probably HCC, LR-5 definitely HCC, LR-M definitely or probably malignant, not HCC specific, LR-TIV tumor in vein.

Abbreviations: AP, arterial phase; MRI, magnetic resonance imaging; LI-RADS, Liver Imaging Reporting and Data System.

$p = 0.029$; Table 8). In the groups with a diameter greater than 50 mm and less than or equal to 100 mm, hepatic capsule retraction, hemorrhage, fat, rim enhancement, dilated vasculature, delayed central enhancement, enhancing capsule, corona enhancement, and LI-M were more frequently observed in the P53-mutated group than in the non-P53-mutated group, although the p value did not reach statistical significance ($p > 0.05$; Table 9).

Table 7 Comparison of Qualitative Data Obtained on MRI Features Stratified by P53 Status (10mm ≤ LTD ≤ 20mm)

MRI Features	Non-P53-Mutated (n =21)	P53-Mutated (n =33)	*p* value
Hypointense at T1-weighted imaging†	18(85.7)	33(100.0)	0.054
Mild-moderate hyperintensity at T2-weighted imaging	21(100.0)	33(100.0)	NA
Hepatic capsule retraction†	0(0)	1(3.0)	1.000
Hemorrhage†	1(4.8)	3(9.1)	1.000
Fat deposition	6(28.6)	9(27.3)	0.917
Diffusion restriction†	19(90.5)	32(97.0)	0.553
Enhancement at AP†			0.298
Nonrim enhancement	18(85.7)	28(84.8)	
Rim enhancement	0(0)	3(9.1)	
Hypoenhanced-isoenhanced	3(14.3)	2(6.1)	
Dilated vasculature at AP dynamic MRI†	4(19.0)	6(18.2)	1.000
Washout at portal venous phase†			0.317
Nonperipheral washout	14(66.7)	25(33.3)	
Peripheral washout	0(0)	2(6.1)	
No washout	7(33.3)	6(18.2)	
Delayed central enhancement†	1(4.8)	0(0)	0.389
Enhancing capsule†	15(71.4)	31(93.9)	0.045
Corona enhancement†	1(4.8)	1(3.0)	1.000
Mosaic architecture†	3(14.3)	6(18.2)	1.000
Nodule-in-nodule architecture†	4(19.0)	7(21.2)	1.000
Tumor in vein	0(0)	0(0)	NA
LI-RADS†			0.190
LR-3	5(23.8)	2(6.0)	
LR-4	1(4.8)	4(12. 1)	
LR-5	14(66.7)	22(66.7)	
LR-M	1(4.8)	5(15.2)	

Notes: The data are presented as the number (%) of patients. †Data were compared using the Fisher's exact test. LR-3 intermediate probability for malignancy, LR-4 probably HCC, LR-5 definitely HCC, LR-M definitely or probably malignant, not HCC specific, LR-TIV tumor in vein, NA, not available.

Abbreviations: AP, arterial phase; MRI, magnetic resonance imaging; LI-RADS, Liver Imaging Reporting and Data System.

Univariate and Multivariate Analyses

Univariate logistic regression analysis identified six risk factors that were significantly related to P53-mutated HCC, namely, largest tumor diameter, AFP level, the Edmondson–Steiner grade, microvascular invasion, rim enhancement, and corona enhancement. These parameters were analysed using multivariate logistic regression. Edmondson–Steiner grade (odds ratio,

Table 8 Comparison of Qualitative Data Obtained on MRI Features Stratified by P53 Status (20mm < LTD ≤ 50mm)

MRI Features	Non-P53-Mutated (n = 91)	P53-Mutated (n = 98)	*p* value
Hypointense at T1-weighted imaging	87(95.6)	92(93.9)	0.749
Mild-moderate hyperintensity at T2-weighted imaging[†]	88(96.7)	95(96.9)	1.000
Hepatic capsule retraction[†]	3(3.3)	8(8.2)	0.216
Hemorrhage	18(19.8)	16(16.3)	0.537
Fat deposition	26(28.6)	34(34.7)	0.366
Diffusion restriction[†]	88(96.7)	91(92.9)	0.334
Enhancement at AP[†]			0.060
Nonrim enhancement	84(92.3)	80(81.6)	
Rim enhancement	7(7.7)	16(16.3)	
Hypoenhanced-isoenhanced	0(0)	2(2.0)	
Dilated vasculature at AP dynamic MRI	58(63.7)	52(53.1)	0.137
Washout at portal venous phase[†]			0.888
Nonperipheral washout	72(79.1)	76(77.6)	
Peripheral washout	4(4.4)	6(6.1)	
No washout	15(16.5)	16(16.3)	
Delayed central enhancement	10(11.0)	7(7.1)	0.356
Enhancing capsule	81(89.0)	88(89.8)	0.861
Corona enhancement	15(16.5)	30(30.6)	0.023
Mosaic architecture	51(56.0)	62(63.3)	0.312
Nodule-in-nodule architecture	14(15.4)	28(28.6)	0.029
Tumor in vein[†]	1(1. 1)	5(5. 1)	0.213
LI-RADS[†]			0.223
LR-3	0(0)	0(0)	
LR-4	4(4.4)	6(6. 1)	
LR-5	71(78.0)	65(66.3)	
LR-M	15(16.5)	22(22.4)	
LR-TIV	1(1. 1)	5(5. 1)	

Notes: The data are presented as the number (%) of patients. [†]Data were compared using the Fisher's exact test. LR-3 intermediate probability for malignancy, LR-4 probably HCC, LR-5 definitely HCC, LR-M definitely or probably malignant, not HCC specific, LR-TIV tumor in vein.

Abbreviations: AP, arterial phase; MRI, magnetic resonance imaging; LI-RADS, Liver Imaging Reporting and Data System.

2.280; 95% CI: 1.268, 4.101; $p = 0.006$) and rim enhancement (odds ratio, 2.517; 95% CI: 1.095, 5.784; $p = 0.030$) were found to be independent variables associated with P53-mutated HCC (Table 10). When the maximum diameter was greater than or equal to 10mm and less than or equal to 20 mm, univariate and multivariate analyses indicated that one risk factor was significantly associated with P53-mutated HCC, and enhancing capsule was an independent predictor of P53-mutated HCC (odds ratio, 6.200;

Table 9 Comparison of Qualitative Data Obtained on MRI Features Stratified by P53 Status (50mm < LTD ≤ 100mm)

MRI features	Non-P53-mutated (n = 36)	P53-mutated (n = 65)	*p* value
Hypointense at T1-weighted imaging†	34(94.4)	65(100.0)	0.125
Mild-moderate at T2-weighted imaging†	36(100.0)	63(96.9)	0.537
Hepatic capsule retraction†	1(2.8)	6(9.2)	0.416
Hemorrhage	15(41.7)	35(53.8)	0.241
Fat deposition	16(44.4)	30(46.2)	0.869
diffusion restriction†	34(94.4)	63(96.9)	0.615
Enhancement at AP†			0.869
Nonrim enhancement	33(91.7)	57(87.7)	
rim enhancement	2(5.6)	6(9.2)	
Hypoenhanced-isoenhanced	1(2.8)	2(3.1)	
Dilated vasculature at AP dynamic MRI	26(72.2)	54(83.1)	0.198
Washout at portal venous phase†			0.202
Nonperipheral washout	31(86.1)	52(80.0)	
peripheral washout	2(5.6)	1(1.5)	
No washout	3(8.3)	12(18.5)	
Delayed central enhancement†	3(8.3)	6(9.2)	1.000
Enhancing capsule†	34(94.4)	62(95.4)	1.000
Corona enhancement	15(41.7)	32(49.2)	0.465
Mosaic architecture†	35(97.2)	61(93.8)	0.653
Nodule-in-nodule architecture	8(22.2)	9(13.8)	0.281
Tumor in vein†	4(11.1)	8(12.3)	1.000
LI-RADS†			1.000
LR-3	0(0)	0(0)	
LR-4	1(2.8)	1(1.5)	
LR-5	26(72.2)	46(70.8)	
LR-M	5(13.9)	10(15.4)	
LR-TIV	4(11.1)	8(12.3)	

Notes: The data are presented as the number (%) of patients. †Data were compared using the Fisher's exact test. LR-3 intermediate probability for malignancy, LR-4 probably HCC, LR-5 definitely HCC, LR-M definitely or probably malignant, not HCC specific, LR-TIV tumor in vein.

Abbreviations: AP, arterial phase; MRI, magnetic resonance imaging; LI-RADS, Liver Imaging Reporting and Data System.

95% CI: 1.116, 34.449; $p = 0.037$; Table 11). When the maximum diameter was between 20 mm and 50 mm, and univariate analysis suggested that Edmondson–Steiner grade, corona enhancement, and nodule-in-nodule architecture were predictors of P53 mutation, and multivariate analysis suggested that corona enhancement (odds ratio, 2.102; 95% CI: 1.022, 4.322; $p = 0.043$) and nodule-in-nodule architecture (odds ratio, 2.157; 95% CI: 1.033, 4.504; $p = 0.041$) were independent risk factors for P53-

Table 10 Univariate and Multivariate Analyses of Risk Factors for the P53-Mutated HCC (10mm ≤ LTD ≤ 100mm)

Risk Factor	Univariate Analysis		Multivariate Analysis	
	Odds Ratio (95% CI)	*p* value	Odds Ratio (95 CI)	*p* value
Age (years)[a]	0.985(0.966–1.003)	0.110		
Sex (male:female)	0.734(0.427–1.261)	0.263		
Largest diameter (mm)[a]	1.012(1.002–1.022)	0.023	1.009(0.997–1.020)	0.151
Alpha-fetoprotein				
Alpha-fetoprotein< 20(ng/mL)*				
Alpha-fetoprotein ≥ 20 and < 400 (ng/mL)	1.050(0.632–1.744)	0.851	0.823(0.478–1.416)	0.482
Alpha-fetoprotein ≥ 400 (ng/mL)	2.283(1.292–4.036)	0.004	1.583(0.853–2.937)	0.146
Cancer antigen 19–9 > 37 (U/mL)	0.679(0.352–1.310)	0.249		
Carcinoembryonic antigen > 5 (ng/mL)	0.741(0.312–1.758)	0.496		
Edmondson–Steiner grade (II:III)	2.588(1.501–4.461)	<0.001	2.280(1.268–4.101)	0.006
Microvascular invasion	1.630(1.036–2.565)	0.035	1.062(0.630–1.790)	0.821
Hepatic capsule retraction	2.983(0.969–9.184)	0.057		
Hemorrhage	1.275(0.777-2.091)	0.336		
Fat deposition	1.236(0.789-1.939)	0.355		
Enhancement at AP				
Nonrim enhancement*				
rim enhancement	2.273(1.026-5.033)	0.043	2.517(1.095-5.784)	0.030
Hypoenhanced-isoenhanced	1.227(0.339-4.438)	0.755	1.306(0.339-5.023)	0.698
Dilated vasculature at AP dynamic MRI	0.909(0.589-1.402)	0.666		
Washout at portal venous phase				
Nonperipheral washout*				
peripheral washout	1. 147(0.397-3.313)	0.800		
No washout	1.040(0.588-1.838)	0.893		
Delayed central enhancement	0.680(0.309-1.494)	0.337		
Enhancing capsule	1.671(0.812-3.437)	0.163		
Corona enhancement	1.788(1.088-2.938)	0.022	1.262(0.724-2. 199)	0.411
Mosaic architecture	1.276(0.820-1.986)	0.279		
Nodule-in-nodule architecture	1.358(0.791-2.331)	0.267		
Tumor in vein	2.032(0.708-5.831)	0.188		
LI-RADS				
LR-3*				
LR-4	4.583(0.673-31. 198)	0.120		

(*Continued*)

Table 10 (Continued).

Risk Factor	Univariate Analysis		Multivariate Analysis	
	Odds Ratio (95% CI)	*p* value	Odds Ratio (95 CI)	*p* value
LR-5	2.995(0.570-15.740)	0.195		
LR-M	4.405(0.785-24. 106)	0.092		
LR-TIV	6.500(0.937-45. 106)	0.058		

Notes: [a]Data are the means ± standard deviations. *Data were used as the reference variable.

Table 11 Univariate and Multivariate Analyses of Risk Factors for the P53-Mutated HCC (10mm ≤ LTD ≤ 20mm)

Risk Factor	Univariate Analysis		Multivariate Analysis	
	Odds Ratio (95% CI)	*p* value	Odds Ratio (95% CI)	*p* value
Age (years)[a]	0.963(0.908–1.022)	0.214		
Sex (male:female)	0.444(0.125–1.578)	0.210		
Largest diameter (mm)	0.947(0.776–1.155)	0.590		
Alpha-fetoprotein				
Alpha-fetoprotein< 20(ng/mL)*				
Alpha-fetoprotein ≥ 20 and < 400 (ng/mL)	2.000(0.585–6.832)	0.269		
Alpha-fetoprotein ≥ 400 (ng/mL)	1.429(0.281–7.261)	0.667		
Cancer antigen 19–9 > 37 (U/mL)	0.387(0.059–2.540)	0.323		
Carcinoembryonic antigen > 5 (ng/mL)	1.290(0.110–15.185)	0.839		
Edmondson–Steiner grade (II:III)	7.500(0.874–64.355)	0.066		
Microvascular invasion	NA	NA		
Hepatic capsule retraction	NA	NA		
Hemorrhage	2.000(0.194-20.614)	0.560		
Fat deposition	0.938(0.277-3. 169)	0.917		
Enhancement at AP				
Nonrim enhancement*				
rim enhancement	NA	NA		
Hypoenhanced-isoenhanced	0.429(0.065-2.822)	0.378		
Dilated vasculature at AP dynamic MRI	0.944(0.232-3.842)	0.936		
Washout at portal venous phase				
Nonperipheral washout*				
peripheral washout	NA	NA		
No washout	0.480(0.135-1.712)	0.258		

(*Continued*)

Table 11 (Continued).

Risk Factor	Univariate Analysis		Multivariate Analysis	
	Odds Ratio (95% CI)	***p* value**	**Odds Ratio (95% CI)**	***p* value**
Delayed central enhancement	NA	NA		
Enhancing capsule	6.200(1.116-34.449)	0.037	6.200(1.116-34.449)	0.037
Corona enhancement	0.625(0.037-10.565)	0.625		
Mosaic architecture	1.333(0.295-6.028)	0.709		
Nodule-in-nodule architecture	1. 144(0.290-4.513)	0.847		
Tumor in vein	NA	NA		
LI-RADS				
LR-3*				
LR-4	10.000(0.648-154.397)	0.099		
LR-5	3.929(0.668-23.097)	0.130		
LR-M	12.500(0.839-186.299)	0.067		

Notes: [a]Data are the means ± standard deviations. *Data were used as the reference variable. NA, not available.

mutated HCC (Table 12). When the maximum diameter was greater than 50 mm and less than or equal to 100 mm, in univariate analysis, the maximum diameter and AFP were associated with P53-mutated HCC, at multivariable regression analysis, increased diameter (odds ratio, 1.035; 95% CI: 1.001, 1.069; $p = 0.044$) and AFP ≥ 400 (ng/mL) (odds ratio, 3.336; 95% CI: 1.052, 10.577; $p = 0.041$) were independent variables associated with P53-mutated HCC (Table 13).

Table 12 Univariate and Multivariate Analyses of Risk Factors for the P53-Mutated HCC (20mm < LTD ≤ 50mm)

Risk factor	Univariate analysis		Multivariate analysis	
	Odds ratio (95% CI)	***p* value**	**Odds ratio (95% CI)**	***p* value**
Age (years)[a]	0.997 (0.973-1.022)	0.831		
Sex (male:female)	0.979(0.470-2.041)	0.956		
Largest diameter (mm)	1.018(0.984-1.053)	0.299		
Alpha-fetoprotein				
Alpha-fetoprotein< 20(ng/ml)*				
Alpha-fetoprotein ≥ 20 and < 400 (ng/ml)	0.997(0.499-1.989)	0.992		
Alpha-fetoprotein ≥ 400 (ng/ml)	1.664(0.784-3.533)	0.185		
Cancer antigen 19-9 > 37 (U/ml)	1.024(0.413-2.540)	0.959		
Carcinoembryonic antigen > 5 (ng/ml)	0.924(0.287-2.975)	0.894		
Edmonson-Steiner grade (II:III)	2.235(1.109-4.505)	0.024	1.949(0.947-4.011)	0.070
Microvascular invasion	1.269(0.684-2.356)	0.450		
Hepatic capsule retraction	2.607(0.670-10.149)	0.167		
Hemorrhage	0.791(0.376-1.665)	0.537		

(*Continued*)

Table 12 (Continued).

Risk factor	Univariate analysis		Multivariate analysis	
	Odds ratio (95% CI)	***p* value**	**Odds ratio (95% CI)**	***p* value**
Fat deposition	1.328(0.717-2.460)	0.367		
Enhancement at AP				
Nonrim enhancement*				
rim enhancement	NA	NA		
Hypoenhanced-isoenhanced	0.429(0.065-2.822)	0.378		
Dilated vasculature at AP dynamic MRI	0.643(0.359-1.152)	0.138		
Washout at portal venous phase				
Nonperipheral washout*				
peripheral washout	1.421(0.385-5.243)	0.598		
No washout	1.011(0.466-2.193)	0.979		
Delayed central enhancement	0.623(0.227-1.713)	0.359		
Enhancing capsule	1.086(0.430-2.745)	0.861		
Corona enhancement	2.235(1.109-4.505)	0.024	2.102(1.022-4.322)	0.043
Mosaic architecture	1.351(0.754-2.420)	0.312		
Nodule-in-nodule architecture	2.200(1.072-4.513)	0.032	2.157(1.033-4.504)	0.041
Tumor in vein	4.839(0.554-42.231)	0.154		
LI-RADS				
LR-4*				
LR-5	0.610(0.165-2.260)	0.460		
LR-M	0.978(0.235-4.066)	0.975		
LR-TIV	3.333(0.276-40.287)	0.344		

Table 13 Univariate and Multivariate Analyses of Risk Factors for the P53-Mutated HCC (50mm < LTD ≤ 100mm)

Risk Factor	Univariate Analysis		Multivariate Analysis	
	Odds Ratio (95% CI)	***p* value**	**Odds Ratio (95% CI)**	***p* value**
Age (years)[a]	0.965(0.929–1.002)	0.066		
Sex (male:female)	0.563(0.196–1.615)	0.285		
Largest diameter (mm)[a]	1.040(1.008–1.073)	0.014	1.035(1.001–1.069)	0.044
Alpha-fetoprotein				
Alpha-fetoprotein< 20(ng/mL)*				
Alpha-fetoprotein ≥ 20 and < 400 (ng/mL)	0.665(0.247–1.791)	0.419	0.618(0.223–1.717)	0.356

(*Continued*)

Table 13 (Continued).

Risk Factor	Univariate Analysis		Multivariate Analysis	
	Odds Ratio (95% CI)	***p* value**	**Odds Ratio (95% CI)**	***p* value**
Alpha-fetoprotein ≥ 400 (ng/mL)	4.032(1.305–12.458)	0.015	3.336(1.052–10.577)	0.041
Cancer antigen 19–9 > 37 (U/mL)	0.422(0.139–1.282)	0.128		
Carcinoembryonic antigen > 5 (ng/mL)	0.387(0.082–1.836)	0.232		
Edmondson–Steiner grade (II:III)	2.558(0.926–7.066)	0.070		
Microvascular invasion	1.708(0.749–3.898)	0.203		
Hepatic capsule retraction	3.559(0.411–30.799)	0.249		
Hemorrhage	1.633(0.717–3.718)	0.242		
Fat deposition	1.071(0.473-2.429)	0.869		
Enhancement at AP				
Nonrim enhancement*				
rim enhancement	1.737(0.331-9. 105)	0.514		
Hypoenhanced-isoenhanced	1. 158(0.101-13.264)	0.906		
Dilated vasculature at AP dynamic MRI	1.888(0.712-5.010)	0.202		
Washout at portal venous phase				
Nonperipheral washout*				
peripheral washout	0.298(0.026-3.424)	0.331		
No washout	2.385(0.624-9. 116)	0.204		
Delayed central enhancement	1. 119(0.262-4.768)	0.880		
Enhancing capsule	1.216(0.194-7.635)	0.835		
Corona enhancement	1.358(0.597-3.088)	0.466		
Mosaic architecture	0.436(0.047-4.054)	0.465		
Nodule-in-nodule architecture	0.563(0.196-1.615)	0.285		
Tumor in vein	1. 123(0.313-4.022)	0.859		
LI-RADS				
LR-4*				
LR-5	1.769(0.106-29.481)	0.691		
LR-M	2.000(0.102-39.079)	0.648		
LR-TIV	2.000(0.098-41.003)	0.653		

Notes: [a]Data are the means ± standard deviations. *Data were used as the reference variable.

Discussion

To date, few studies have analysed the sensitivity or specificity of MRI features for diagnosing or predicting the clinical outcome of P53-mutated HCC. In our study, several of the imaging features were related to P53-mutated HCC; P53-

mutated HCC was associated with poorer differentiation and was more likely to show peripheral rim-like enhancement on imaging. In patients with small HCC (10 mm ≤ LTD ≤ 20 mm), enhancing capsule was an independent predictor of P53-mutated HCC; in lesions with a diameter ranging from 20 mm to 50 mm, corona enhancement and nodule-in-nodule architecture were more likely to be observed in the images of P53-mutated HCC; and in patients with large HCC (50 mm < LTD ≤ 100 mm), a higher serum AFP level and large tumors may indicate a higher risk of P53-mutated HCC, while MRI features showed little difference.

A recent study showed that HCC with peripheral rim-like enhancement is associated with poor differentiation, a high frequency of macrotrabecular-massive type, and greater susceptibility to microvascular invasion, and peripheral rim-like enhancement is accompanied by increased necrotic areas in the centre of the tumor and frequent expression of the hypoxia-related marker CAIX.[14] Both oncogenes and hypoxia can induce damage to DNA and signal activation in p53.[4] Based on the findings of previous studies, a high degree of rim enhancement suggests that the tumor is highly malignant and poorly differentiated, which increases the rate of early recurrence after curative resection of HCC, and substantial tumor necrosis leads to a poorer prognosis.[15,16] All of these findings are related to the increased malignancy and excessive growth of tumors, and the acquisition of P53 mutants, a transcription factor, promotes metabolic reprogramming of tumors, causing survival and proliferation of tumor cells.[17] In the present study, poor differentiation and arterial-phase ring enhancement on MRI images were risk factors for P53-mutated HCC, and the results were consistent with these findings.

From 1996 to 2007, the Japanese surveillance system showed a yearly increase in the incidence of small HCCs ≤2 cm,[18] and the treatment modalities used were diverse; therefore, understanding the internal characteristics of small HCC can aid in the development of personalized management. In our study, enhancing capsule was a risk factor for P53-mutated HCC in patients with small HCC. Enhancing capsule of HCC in patients with chronic liver disease is more easily recognized in the late portal venous phase of gadoxetic acid disodium-enhanced MRI.[19] The presence of an enhancing capsule in HCC is caused by slow flow within intracapsular vessels and retention of contrast media in prominent peritumoral sinusoidal spaces or fibrosis.[20] Some scholars have shown that the fibrous capsule and the prominent blood sinus overlap, that some microvessels form within the fibrous capsule, that the fibrous capsule accompanies the growth of HCC and that angiogenesis occurs.[21] Recent studies have reported that dilated vessels in a pattern of vessel-encapsulated tumor clusters, possibly corresponding to neovascularized arteries or dilated sinusoidal gaps, are frequently observed on dynamic CT in P53-mutated HCC,[12] and enhancing capsule is a risk factor for the development of microvascular invasion in HCC.[22] Our study demonstrated a close relationship between enhancing capsule and p53-mutated HCC.

Several scholars have studied the preoperative imaging features of solitary HCC (≤5 cm) to identify potential biomarkers that can be appropriately selected to expand the scope of surgical resection and reduce tumor recurrence.[22] Corona enhancement is an important ancillary feature of malignancy in LI-RADS and is readily observed in the late arterial and early portal vein phases. The nodule-in-nodule architecture appears mainly because of the morphological proliferation of poorly differentiated cells in the inner nodes replacing the well-differentiated outer nodes. In our study, P53-mutated HCC lesions with diameters ranging from 20 mm to 50 mm exhibited these imaging features because P53 mutation induced these phenotypes. The internal lesions of HCC may accumulate fat,[23] thus leading to T2 isointense or hyperintense nodules, whereas mutant p53 can promote lipid synthesis by altering the activity of various transcription factors or signalling molecules involved in lipid metabolism, such as p63, p73, Nrf2, and AMP-activated protein kinase (AMPK).[24–26] Neovascularization occurs mainly at the periphery of the tumor and is prone to peripheral corona enhancement, which correlates with corona enhancement due to the rapid decrease in central perfusion, which favours central tumor necrosis and may result in the formation of nodule-in-nodule architecture.[27] Our study identified both nodule-in-nodule architecture and corona enhancement as risk factors for P53-mutated HCC.

In this study, larger HCC (50 mm < LTD ≤ 100 mm) had diverse imaging features, while tumor diameter and AFP level were risk factors for P53-mutated HCC. Rapidly growing HCC usually exhibits areas of necrosis due to hypoxia;[26] thus, larger tumors are prone to cystic degeneration and necrosis, and their imaging features can be affected. Liu et al[28,29] suggesting that increased tumor aggressiveness and infiltrative growth in HCC are associated with larger tumor sizes. P53

is a tumor suppressor gene, but mutant p53 proteins not only lose their tumor suppressor function but also often promote tumorigenesis through various pathways. Larger tumor diameters and AFP levels also negatively affect the survival of HCC patients.[30] AFP can be routinely monitored in patients undergoing HCC surveillance because it is an easily available biomarker for HCC. Elevated serum AFP levels indicate a poor prognosis in patients with HCC.[31] P53 mutations promote hepatocellular carcinoma cell proliferation, and AFP is activated during liver regeneration and hepatocarcinogenesis.[32] Therefore, elevated AFP levels are prone to occur in patients with P53-mutated HCC. Vessel-encapsulated tumor clusters (VETC) promote HCC progression and metastasis; for example, one study indicated that 75% of HCC presenting with VETC were larger than 5 cm in diameter, suggesting that this specific vascular pattern is associated with tumor progression,[33] and other studies have demonstrated that CD34-positive vessel-encapsulating tumor clusters are also more likely to be present in P53-mutated HCC.[12] This study also suggested that larger tumor diameters and higher AFP levels are also more likely to be found in P53-mutated HCC patients.

This study has several limitations. First, because this was a single-centre and retrospective study, selection bias was inevitable. Second, we considered that the immunohistochemical expression of P53 indicated a mutation in *TP*53 (based on the percentage of nuclear staining), which should be confirmed by genomic mapping to improve the accuracy of the results. Third, the tumors in this study were single masses ranging from 10 mm to 100 mm in diameter, and the results cannot be applied to tumors of other diameters or multiple masses. Finally, although preoperative imaging data for P53-mutated HCC patients were obtained, long-term follow-up data are needed to determine the association between outcome and survival.

Conclusion

In conclusion, poor differentiation and rim enhancement on enhanced MRI are useful imaging markers for the diagnosis of P53-mutated HCC. The presence of an enhancing capsule in small HCC (10mm ≤ LTD ≤ 20 mm) can predict P53-mutated HCC, and the presence of corona enhancement and nodule-in-nodule architecture in HCCs with diameters ranging from 20 mm to 50 mm should be highly important for identifying P53-mutated HCC. In large HCC lesions (50 mm < LTD ≤ 100 mm), elevated AFP and enlarged masses should also be emphasized.

Abbreviations

HCC, Hepatocellular carcinoma; MRI, Magnetic Resonance Imaging; LI-RADS, Liver Imaging Reporting and Data System; AFP, Alpha-fetoprotein; CEA, Carcinoembryonic antigen; CA19–9, Cancer antigen 19–9; LTD, The largest tumor diameter; DWI, Diffusion-weighted imaging; LR-M, Probably or definitely malignant, not HCC specific; VETC, Vessel-encapsulating tumor cluster.

Acknowledgments

The authors would like to thank all participants for their valuable support in this study.

Funding

This work was supported by Shanghai Municipal Health Commission (grant number 202240152); Science and Technology Commission of Shanghai Municipality (grant number 23Y11907400).

Disclosure

The authors report no conflicts of interest in this work.

References

1. van Meer S, de Man RA, Coenraad MJ, et al. Surveillance for hepatocellular carcinoma is associated with increased survival: results from a large cohort in the Netherlands. *J Hepatol*. 2015;63(5):1156–1163. doi:10.1016/j.jhep.2015.06.012
2. Kulik L, El-Serag HB. Epidemiology and management of hepatocellular carcinoma. *Gastroenterol*. 2019;156(2):477–491.e1. doi:10.1053/j.gastro.2018.08.065
3. Wu H, Chen X, Chen J, et al. Correlations between P53 mutation status and texture features of ct images for hepatocellular carcinoma. *Methods Inf Med*. 2019;58(1):42–49. doi:10.1055/s-0039-1688758
4. Bargonetti J, Manfredi JJ. Multiple roles of the tumor suppressor p53. *Curr Opin Oncol*. 2002;14(1):86–91. doi:10.1097/00001622-200201000-00015

5. Yuan RH, Jeng YM, Hu RH, et al. Role of p53 and β-catenin mutations in conjunction with CK19 expression on early tumor recurrence and prognosis of hepatocellular carcinoma. *J Gastrointest Surg*. 2011;15(2):321–329. doi:10.1007/s11605-010-1373-x
6. Rebouissou S, Nault JC. Advances in molecular classification and precision oncology in hepatocellular carcinoma. *J Hepatol*. 2020;72(2):215–229. doi:10.1016/j.jhep.2019.08.017
7. Cheng J, Wang W, Sun C, Li M, Wang B, Lv Y. Meta-analysis of the prognostic and diagnostic significance of serum/plasma osteopontin in hepatocellular carcinoma. *J Clin Gastroenterol*. 2014;48(9):806–814. doi:10.1097/MCG.0000000000000018
8. Roayaie S, Obeidat K, Sposito C, et al. Resection of hepatocellular cancer ≤2 cm: results from two Western centers. *Hepatol*. 2013;57(4):1426–1435. doi:10.1002/hep.25832
9. Heimbach JK. Evolution of liver transplant selection criteria and U.S. allocation policy for patients with hepatocellular carcinoma. *Semin Liver Dis*. 2020;40(4):358–364. doi:10.1055/s-0040-1709492
10. Mazzaferro V, Regalia E, Doci R, et al. Liver transplantation for the treatment of small hepatocellular carcinomas in patients with cirrhosis. *N Engl J Med*. 1996;334(11):693–699. doi:10.1056/NEJM199603143341104
11. Sugawara Y, Hibi T. Surgical treatment of hepatocellular carcinoma. *Biosci Trends*. 2021;15(3):138–141. doi:10.5582/bst.2021.01094
12. Kitao A, Matsui O, Zhang Y, et al. Dynamic CT and Gadoxetic Acid-enhanced MRI characteristics of p53-mutated hepatocellular carcinoma. *Radiol*. 2023;306(2):e220531. doi:10.1148/radiol.220531
13. Tseng PL, Tai MH, Huang CC, et al. Overexpression of VEGF is associated with positive p53 immunostaining in hepatocellular carcinoma (HCC) and adverse outcome of HCC patients. *J Surg Oncol*. 2008;98(5):349–357. doi:10.1002/jso.21109
14. Rhee H, An C, Kim HY, Yoo JE, Park YN, Kim MJ. Hepatocellular carcinoma with irregular rim-like arterial phase hyperenhancement: more aggressive pathologic features. *Liver Cancer*. 2019;8(1):24–40.doi:10.1159/000488540.
15. An C, Kim DW, Park YN, Chung YE, Rhee H, Kim MJ. Single Hepatocellular Carcinoma: preoperative MR imaging to predict early recurrence after curative resection. *Radiol*. 2015;276(2):433–443. doi:10.1148/radiol.15142394
16. Nakachi K, Tamai H, Mori Y, et al. Prediction of poorly differentiated hepatocellular carcinoma using contrast computed tomography. *Cancer Imag*. 2014;14(1):7. doi:10.1186/1470-7330-14-7
17. Yu L, Wu M, Zhu G, Xu Y. Emerging roles of the tumor suppressor p53 in metabolism. *Front Cell Dev Biol*. 2022;9:762742. doi:10.3389/fcell.2021.762742
18. Takayasu K, Arii S, Sakamoto M, et al. Impact of resection and ablation for single hypovascular hepatocellular carcinoma ≤2 cm analysed with propensity score weighting. *Liver Int*. 2018;38(3):484–493. doi:10.1111/liv.13670
19. Kim H, Kim SS, Shin HC, et al. Gadoxetate disodium-enhanced MRI for diagnosis of hepatocellular carcinoma in patients with chronic liver disease: late portal venous phase may improve identification of enhancing capsule. *Abdom Radiol (NY)*. 2023;48(2):621–629. doi:10.1007/s00261-022-03756-2
20. Choi JY, Lee JM, Sirlin CB. CT and MR imaging diagnosis and staging of hepatocellular carcinoma: part II. Extracellular agents, hepatobiliary agents, and ancillary imaging features. *Radiol*. 2014;273(1):30–50. doi:10.1148/radiol.14132362
21. Iguchi T, Aishima S, Sanefuji K, et al. Both fibrous capsule formation and extracapsular penetration are powerful predictors of poor survival in human hepatocellular carcinoma: a histological assessment of 365 patients in Japan. *Ann Surg Oncol*. 2009;16(9):2539–2546. doi:10.1245/s10434-009-0453-1
22. Chong HH, Yang L, Sheng RF, et al. Multi-scale and multi-parametric radiomics of gadoxetate disodium-enhanced MRI predicts microvascular invasion and outcome in patients with solitary hepatocellular carcinoma ≤ 5 cm. *Eur Radiol*. 2021;31(7):4824–4838. doi:10.1007/s00330-020-07601-2
23. Sano K, Ichikawa T, Motosugi U, et al. Imaging study of early hepatocellular carcinoma: usefulness of gadoxetic acid-enhanced MR imaging. *Radiol*. 2011;261(3):834–844. doi:10.1148/radiol.11101840
24. Do PM, Varanasi L, Fan S, et al. Mutant p53 cooperates with ETS2 to promote etoposide resistance. *Genes Dev*. 2012;26(8):830–845. doi:10.1101/gad.181685.111
25. Walerych D, Lisek K, Sommaggio R, et al. Proteasome machinery is instrumental in a common gain-of-function program of the p53 missense mutants in cancer. *Nat Cell Biol*. 2016;18(8):897–909. doi:10.1038/ncb3380
26. Xu J, Reumers J, Couceiro JR, et al. Gain of function of mutant p53 by coaggregation with multiple tumor suppressors. *Nat Chem Biol*. 2011;7(5):285–295. doi:10.1038/nchembio.546
27. Tohme S, Yazdani HO, Liu Y, et al. Hypoxia mediates mitochondrial biogenesis in hepatocellular carcinoma to promote tumor growth through HMGB1 and TLR9 interaction. *Hepatol*. 2017;66(1):182–197. doi:10.1002/hep.29184
28. Liu HF, Wang M, Wang Q, et al. Multiparametric MRI-based intratumoral and peritumoral radiomics for predicting the pathological differentiation of hepatocellular carcinoma. *Insights Imag*. 2024;15(1):97. doi:10.1186/s13244-024-01623-w
29. Liu HF, Lu Y, Wang Q, Lu YJ, Xing W. Machine Learning-Based CEMRI radiomics integrating LI-RADS features achieves optimal evaluation of hepatocellular carcinoma differentiation. *J Hepatocell Carcinoma*. 2023;10:2103–2115. doi:10.2147/JHC.S434895
30. Renne SL, Woo HY, Allegra S, et al. Vessels encapsulating tumor clusters (VETC) is a powerful predictor of aggressive hepatocellular carcinoma. *Hepatol*. 2020;71(1):183–195. doi:10.1002/hep.30814
31. Montal R, Andreu-Oller C, Bassaganyas L, et al. Molecular portrait of high alpha-fetoprotein in hepatocellular carcinoma: implications for biomarker-driven clinical trials. *Br J Cancer*. 2019;121(4):340–343. doi:10.1038/s41416-019-0513-7
32. Yamashita T, Kitao A, Matsui O, et al. Gd-EOB-DTPA-enhanced magnetic resonance imaging and alpha-fetoprotein predict prognosis of early-stage hepatocellular carcinoma. *Hepatol*. 2014;60(5):1674–1685. doi:10.1002/hep.27093
33. Fang JH, Zhou HC, Zhang C, et al. A novel vascular pattern promotes metastasis of hepatocellular carcinoma in an epithelial-mesenchymal transition-independent manner. *Hepatol*. 2015;62(2):452–465. doi:10.1002/hep.27760